

Accuracy of cardiac-induced brain motion measurement using displacement-encoding with stimulated echoes (DENSE) magnetic resonance imaging (MRI): A phantom study

Blaise Simplicie Talla Nwotchouang¹   | Maggie S. Eppelheimer¹ | Dipankar Biswas² | Soroush Heidari Pahlavian³ | Xiaodong Zhong⁴  | John N. Oshinski⁵ | Daniel L. Barrow⁶ | Rouzbeh Amini⁷ | Francis Loth^{1,8}

¹Conquer Chiari Research Center, Department of Biomedical Engineering, The University of Akron, Akron, Ohio, USA

²Fluids and Structure (FaST) Laboratory, Department of Mechanical and Aerospace Engineering, University of Central Florida, Orlando, Florida, USA

³Laboratory of FMRI Technology (LOFT), USC Stevens Neuroimaging and Informatics Institute, University of Southern California, Los Angeles, California, USA

⁴Siemens Healthcare, Los Angeles, California, USA

⁵Radiology & Imaging Sciences and Biomedical Engineering, Emory University School of Medicine, Atlanta, Georgia, USA

⁶Department of Neurosurgery, Emory University, Atlanta, Georgia, USA

⁷Department of Mechanical and Industrial Engineering, Department of Bioengineering, Northeastern University, Boston, Massachusetts, USA

⁸Department of Mechanical Engineering, The University of Akron, Akron, Ohio, USA

Correspondence

Blaise Simplicie Talla Nwotchouang,
Conquer Chiari Research Center, The
University of Akron, 264 Wolf Ledges
Pkwy #211B, Akron, OH 44325, USA.
Email: bn23@zips.uakron.edu

Funding information

Conquer Chiari; the National Institutes of Health, NINDS R15 (Grant No. 1R15NS109957-01A1); the National Center for Advancing Translational Sciences of the National Institutes of Health (Award No: UL1TR002378); and the National Science Foundation (NSF CAREER Award No. 1846715).

Purpose: The goal of this study was to determine the accuracy of displacement-encoding with stimulated echoes (DENSE) MRI in a tissue motion phantom with displacements representative of those observed in human brain tissue.

Methods: The phantom was comprised of a plastic shaft rotated at a constant speed. The rotational motion was converted to a vertical displacement through a camshaft. The phantom generated repeatable cyclical displacement waveforms with a peak displacement ranging from 92 μm to 1.04 mm at 1-Hz frequency. The surface displacement of the tissue was obtained using a laser Doppler vibrometer (LDV) before and after the DENSE MRI scans to check for repeatability. The accuracy of DENSE MRI displacement was assessed by comparing the laser Doppler vibrometer and DENSE MRI waveforms.

Results: Laser Doppler vibrometer measurements of the tissue motion demonstrated excellent cycle-to-cycle repeatability with a maximum root mean square error of 9 μm between the ensemble-averaged displacement waveform and the individual waveforms over 180 cycles. The maximum difference between DENSE MRI and the laser Doppler vibrometer waveforms ranged from 15 to 50 μm . Additionally, the peak-to-peak difference between the 2 waveforms ranged from 1 to 18 μm .

Conclusion: Using a tissue phantom undergoing cyclical motion, we demonstrated the percent accuracy of DENSE MRI to measure displacement similar to that observed for in vivo cardiac-induced brain tissue.

KEYWORDS

cardiac-induced brain tissue displacement, displacement-encoding with stimulated echoes magnetic resonance imaging, laser Doppler vibrometer, phantom, validation

1 | INTRODUCTION

Displacement encoding with stimulated echoes (DENSE) is an MRI sequence where displacement is encoded into the phase of the MR signal.^{1,2} DENSE MRI was initially developed by Aletras et al to quantify cardiac tissue biomechanics.¹ The technique was extended to a cine sequence by Kim et al,³ and a spiral version of the technique was developed by Zhong et al.^{2,4} In multiple studies, myocardial and vascular tissue biomechanics were examined using DENSE MRI.²⁻⁷ The DENSE sequence involves 2 modules: a displacement-encoding module and an imaging module. The displacement-encoding module tips the longitudinal magnetization into the transverse plane, encodes the tissue motion into the phase of the magnetization, and then restores the magnetization back to the longitudinal axis. The imaging module consists of multiframe (cine) acquisition using a fast imaging sequence with a small flip angle (FA). The imaging module contains an unencoding gradient to rewind the phase, so that only displacement-related phase shifts are present in the phase of the data for each frame.

Cardiac and respiratory cycles induce pulsatile brain tissue motion.^{8,9} Using phase-contrast imaging, Reese et al was the first to demonstrate that brain tissue strain can be quantified noninvasively.¹⁰ In 2009, Soellinger et al and Zhong et al showed that the DENSE MRI technique can be used to quantify cardiac-induced brain tissue motion.^{4,11} In 2018, Pahlavian et al quantified regional brain tissue displacement and strain in healthy subjects using DENSE MRI.¹² Adams et al determined cardiac-induced brain tissue expansion using DENSE MRI and demonstrated that tissue-specific volumetric strain quantification was possible with DENSE.¹³ Also, Adams et al reported that cerebral pulsatility between intersubjects showed a consistent peak value and was also strongly correlated to cerebrospinal fluid flow volume changes in healthy subjects.¹⁴ Recently, in a study to determine cardiac- and respiratory-induced brain deformation using a novel high-field MRI, Sloots et al determined that the heartbeat-induced volumetric strain was 3 times larger than respiratory-induced volumetric strain, which was determined using an optimal tag spacing of 0.15 mm/π.¹⁵ These studies have demonstrated the feasibility of DENSE MRI to quantify brain tissue displacement and strain. However, the accuracy of DENSE-measured brain tissue displacement has not been reported.

Previous phantom studies have validated displacement derived from velocity-encoding techniques.¹⁶⁻¹⁸ Displacement

derived from phase-contrast magnetic resonance imaging (PCMRI) has been used to quantify neural tissue displacement.^{8,19-26} Several efforts have been made to validate the myocardium displacement measurement obtained from DENSE MRI.^{3,27-29} Spottiswoode et al compared myocardial displacement measured by DENSE with known displacements in a rigid rotating phantom and reported a 240 ± 150 -μm displacement error in the accuracy of the tracking algorithm for displacement values typical of cardiac displacement.²⁷ Although studies have sought to validate DENSE MRI measurements for the relatively large values of myocardial motion, DENSE MRI has not been validated for cardiac-induced brain tissue displacement, which is far lower in magnitude compared with myocardial motion. The maximum displacement reported in the myocardium is 6 to 10 mm,³⁰ whereas the maximum displacement reported in the brain by Pahlavian et al and Adams et al was 187-100 μm, respectively.^{12,13} The reported displacement in brain tissue is lower than the error reported in the accuracy study of DENSE MRI for myocardial motion by Spottiswoode et al.²⁷ As such, a validation study is of paramount importance to determine if DENSE MRI is capable of accurately quantifying brain tissue motion below 200 μm.

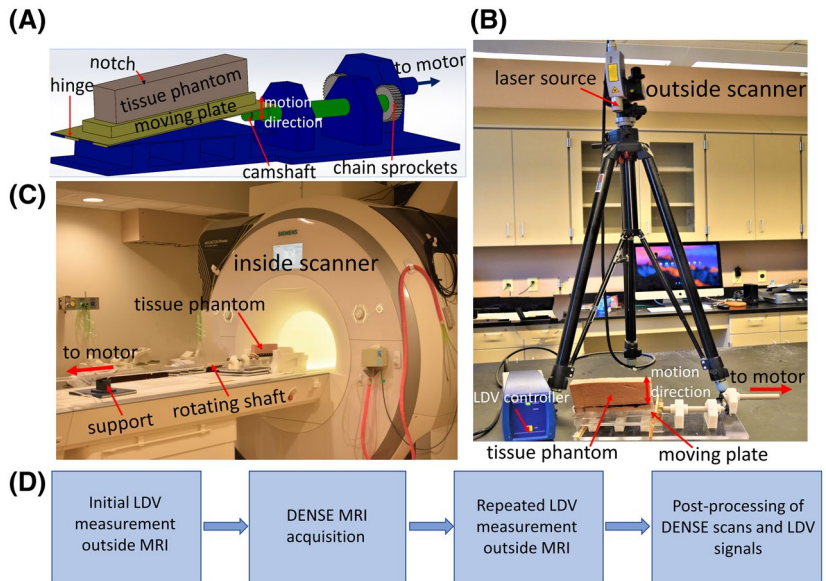
The goal of this study was to determine the accuracy of cine spiral DENSE MRI for the measurement of displacement in a tissue phantom with displacements representative of those observed in human brain tissue. An experimental cyclic displacement device was developed that generated tissue phantom motion representative of displacement observed in human brain tissue. The reference values for the phantom displacement waveform were determined with a laser Doppler vibrometer (LDV) and were compared with the DENSE MRI displacement measurements. Additionally, the effect of voxel averaging on the accuracy of displacement measurements was examined.

2 | METHODS

2.1 | Cyclic displacement device

An in vitro cyclical displacement device was developed at The University of Akron to generate a repeatable displacement waveform similar in magnitude and shape to that of in vivo cardiac-induced brain tissue motion (Figure 1A). A high-torque rotary motor (respiration pump speed control, model number: H0156023; Harvard Apparatus, Holliston, MA) was

FIGURE 1 A, Set-up for the moving plate showing the location of the notch on tissue phantom, B, laser Doppler vibrometer (LDV) measurement outside the scanner. C, Displacement-encoding with stimulated echoes magnetic resonance imaging (DENSE MRI) measurement. D, Sequential steps to acquire LDV measurements and DENSE scans



used to drive a camshaft at a constant rotational speed of 60 cycles per minute. A 304-cm-long, clear polyethylene terephthalate tube was used to connect the rotating motor to a roller chain sprocket that drives the camshaft. Two miniature roller chain sprockets were used to separate the connection between the driveshaft and the camshaft to minimize vibrations from the electric motor (Figure 1A). The camshaft was made from a plastic rod (polyether ether ketone) that was 1.9 cm in diameter. The moving plate was 0.625-cm thick, 25-cm long, and 10-cm wide, and was made from a clear cast acrylic sheet. A 1.04-mm cyclic peak displacement was generated by a rotating asymmetric camshaft at the end of the plate. The camshaft converted the rotational motion of the motor to an approximate up-and-down motion of the plate at one end, such that the plate motion was rotational about a hinge at the opposite end. The distance from the hinge center to the camshaft was 24 cm. Thus, the moving plate only rotated through an angle of $<1^\circ$ for a 1.04-mm vertical displacement with zero displacements at the hinge. All components for the moving plate were obtained from McMaster-Carr (Elmhurst, IL).

2.2 | LDV set-up and external trigger development

A fiber-coupled LDV device (model OFV-534; Polytec Holding AG, Hürsching, Austria) that was capable of detecting velocities as low as $1 \mu\text{m/s}$ was used to determine the tissue phantom displacement LDV reference waveform (see Figure 1B). The tissue phantom consisted of a block of pre-cooked meat (bologna obtained from a local market; see Figure 1B) with a height of 83 mm and a width of 38 mm. Using a scalpel, a notch was created on the tissue phantom as a fiducial marker to identify the location of the LDV measurement on the MRI scan (see Figure 1A for the location of the

notch on the tissue phantom). For the LDV and MRI measurements, an external trigger was used to determine the precise start and endpoint of each waveform. In human DENSE MRI measurements, the acquisition begins once changes in physiological events are detected (for example, an R-wave or a peak peripheral pulse measured at the index finger). In our cyclic displacement device, an external trigger was used in place of the R-wave to signal the start of the MRI data acquisition process. A 5-V square wave with a pulse width of 70 ms was sent to the MRI scanner through a Bayonet Neill–Concelman cable. The external trigger was developed with an infrared obstacle avoidance device (DASAN Zhone Solutions [DZS], Plano, TX). The device consisted of a pair of infrared transmitting and receiving sensors. An Arduino Uno (Arduino LLC, Boston, MA) was used to control the voltage (5 V) supplied to the device. A 0.625-cm-wide plastic obstacle was attached to the rotating pipe and placed at a distance of 5 cm from the infrared sensor. In this set-up, the 5-V square-wave signal was generated at a given time point in each cycle when the plastic obstacle blocks the infrared beam received by the sensor; however, no voltage is generated if the infrared beam reaches the sensor. The trigger signal from the Arduino and the velocity signal from the LDV were acquired using a National Instruments data acquisition board (NI-USB-6259; National Instruments, Austin, TX). Postprocessing of the signals was performed using an in-house program developed in MATLAB 2018b (MathWorks, Natick, MA).

2.3 | Experimental procedure

All measurements were performed at the Center for Systems Imaging, located at the Emory University School of Medicine (Figure 1C; Atlanta, GA). The LDV measurements were obtained before and after MRI acquisition

outside the scanner room (Figure 1D). The LDV device was activated 20 minutes prior to the first experiment to allow time for the helium-neon laser head to reach thermal equilibrium. Polytec A-RET-T010 retroreflective tape (Polytec, Inc, Dexter, MI) was attached to the tissue phantom at 4 different distances from the hinge (11.8, 30.9, 45.0, and 62.1 mm from the hinge). The LDV measurements were collected at 60 cycles per minute for 180 seconds with a sampling frequency of 40 kHz. LDV measurements were acquired before and after the DENSE MRI measurements to document the repeatability of the cyclic displacement device because the movement of the device into and out of the MR scanner required disconnection/reconnection of the long rotating shaft.

2.4 | DENSE MRI acquisition protocol

Sagittal images of the tissue phantom were acquired on a 3T MRI scanner (PrismaFit; Siemens Healthcare, Erlangen, Germany), using a 20-channel head coil. The magnitude and displacement-encoded phase images were acquired using the sequence outlined in previous studies.^{2,4,12} The DENSE sequence was modified by adjusting the encoding frequency (k_e) to 0.6 cycles/mm to minimize phase wrap. A simple encoding scheme was used and through-plane dephasing at a frequency of 0.8 mm/cycle was used to suppress T_1 relaxation echoes.³¹ The DENSE MRI acquisition was initialized after the MRI detected the external 5-V signal supplied from the trigger. Thirty frames were obtained during the simulated cardiac cycle (period of 1 second) with the temporal resolution of 34 ms. The time to encode the displacement (displacement-encoding module time) before the first cardiac phase was 4 ms. The slice thickness was 8 mm, the field of view was 250×250 , and the matrix was 256×256 , yielding a pixel size of $0.9 \text{ mm} \times 0.9 \text{ mm}$. The readout of the DENSE images was an interleaved spiral acquisition; the number of spiral interleaves was 26; and the duration of each spiral interleave was 16 ms. The echo time of the sequence was 2.2 ms; the FA was 15° ; and a volume shim over the field of view was utilized. The total scan time was 3 minutes. DENSE MR images were also acquired when the motor was turned off to assess the effect of noise and background phase on the displacement measurements.

2.5 | Postprocessing of LDV signals

Postprocessing of the velocity signal from the LDV was performed with an in-house program developed in MATLAB. Measurements of the plate velocity with the motor off (ie, plate not moving) were consistently 0.014 mm/s over the 180-second period; this was designated as the velocity measurement offset of the LDV system. Thus, LDV velocity

measurements were corrected by subtracting this consistent offset measurement error from all LDV measurements to ensure the same start and end location of the displacement waveform. One cycle at the start and end of the measurement period was discarded to eliminate any start/stop effects. A threshold of 4.5 V was used to determine the rising edges of the trigger signal (the start of the velocity waveform) and to separate the velocity waveform into 180 individual waveforms (Figure 2A). The cumulative trapezoidal numerical integration method was used to integrate the individual velocity waveforms to obtain the individual displacement waveforms. An ensemble average displacement reference waveform was then computed from the individual displacement waveforms. To quantify the cycle-to-cycle displacement errors, the ensemble average displacement reference waveform was compared with the 180 individual displacement waveforms (Figure 2B). The minimum, maximum cycle-to-cycle difference, and the root mean square error (RMSE) were determined between the ensemble average and the individual waveforms. To determine the disconnection/reconnection repeatability, metrics from 2 ensemble average displacement reference waveforms (before and after DENSE MRI measurements) were compared, including peak-to-peak difference, range of difference (minimum and maximum difference), and the RMSE. To examine additional locations on the tissue phantom, we extrapolated the linear fit of the 4 LDV measurements to obtain an estimated LDV (e-LDV) measurement across the tissue's superior-inferior length.

2.6 | Postprocessing of DENSE scans

A custom-made program developed in MATLAB was used to postprocess the DENSE image sets (Figure 3A-D). The steps used to obtain the DENSE MRI displacement were similar to those described by Pahlavian et al.¹² The DENSE-measured displacements were calculated after phase-unwrapping (if necessary), noise-filtering, and selecting regions of interest (Figure 3A-C).¹² Noise-filtering was performed using the `filter2` function in MATLAB 2018b. This function applied a finite impulse response filter to the displacement measurement. The values of the normalized cut-off frequency and filter order was 0.15 and 16, respectively, as recommended by Pahlavian et al.¹² For each phase image, pixelwise 2-dimensional Eulerian displacement maps were created for the selected regions of interest (see Figure 3D). For each time point, 80 voxels with displacement values were averaged (from the anterior to the posterior section of the tissue phantom; from left to right in Figure 3B) to obtain the final MRI displacement waveform. We were able to perform such procedures as our experimental system was designed in such a way that in each one of these images, the displacement of all averaged voxels was theoretically the same (see Supporting Information Figure S1).

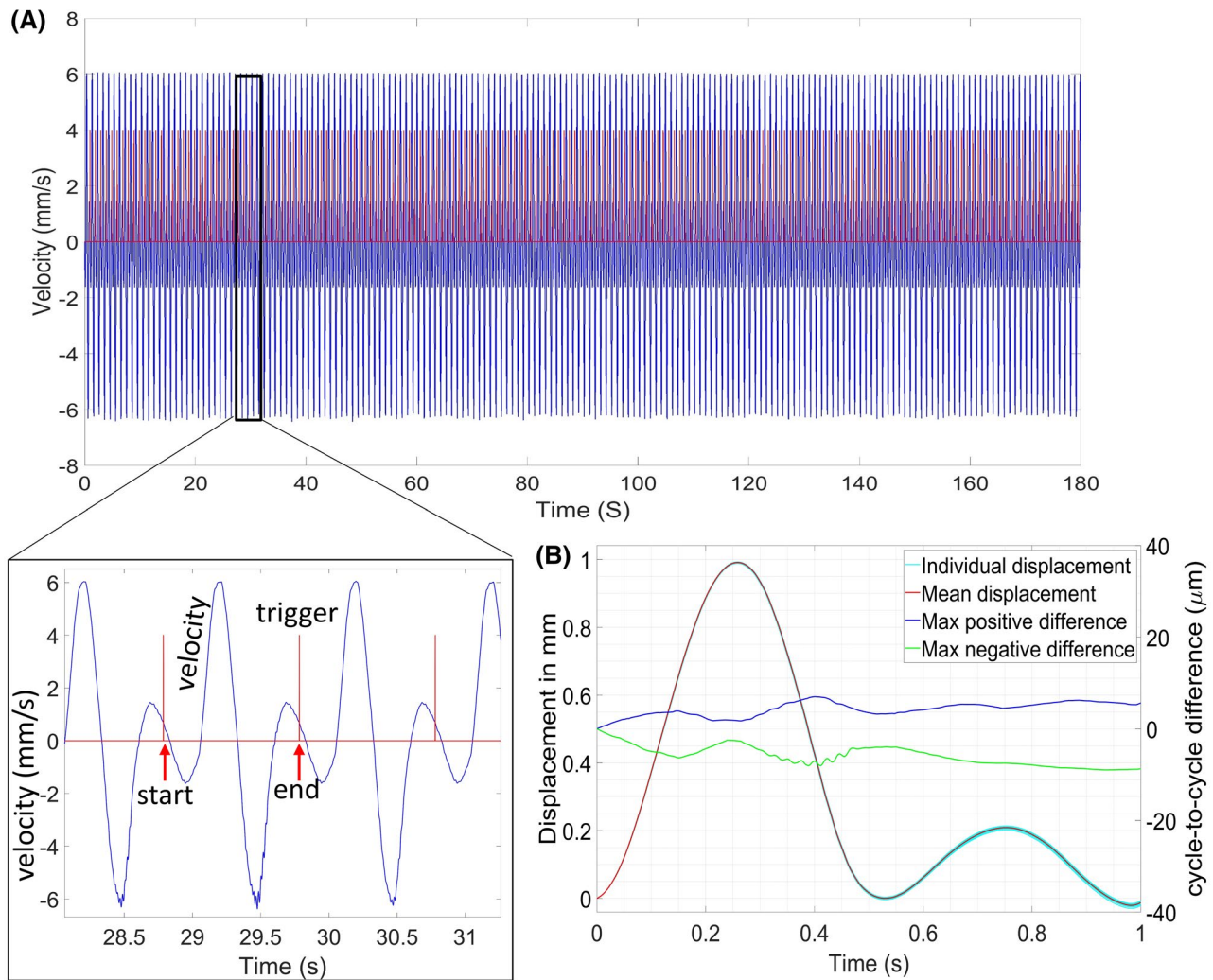


FIGURE 2 Steps used to validate the cycle-to-cycle consistency of the displacement cyclic device. A, Velocity and trigger waveforms (insert shows the start and stop locations of each velocity waveform). B, Mean and individual displacement waveforms obtained after integrating the velocity waveform. Note: All 180 displacement waveforms are superimposed upon one another. The blue and green lines represent the maximum positive and negative differences between the mean and all 180 individual waveforms, respectively—and obtained by subtracting the individual waveforms from the mean. These 2 waveforms were plotted on the right y-axis

The DENSE scans with no plate motion showed an average displacement of $3 \pm 6 \mu\text{m}$, suggesting that the background offset had a minimal impact on the overall MRI-measured displacement waveform. As such, no background offset correction was performed for DENSE measurements in the present study.

The DENSE MRI displacement waveform and the LDV ensemble-averaged displacement reference waveforms were shifted in time such that the peak systole was at the beginning of the waveform. Also, the waveforms were adjusted to ensure that the 2 waveforms (LDV reference and DENSE MRI) started from the origin (0,0). This was done to make sure that the 2 waveforms have a similar starting point prior to comparison. The following parameters were computed between the 2 waveforms: peak-to-peak difference, range of difference (minimum and maximum difference), and RMSE. Additionally, we examined the effect of

averaging on a collection of contiguous voxels on the accuracy of the displacement measurement for the peak-to-peak difference between DENSE MRI and LDV displacement waveforms. Voxel averaging was performed across the sagittal plane in the anterior–posterior direction for 40, 20, 10, 5, and 2 contiguous voxels (white line #1-4 in Figure 3B). Waveforms were computed using the average values for 40, 20, 10, 5, and 2 contiguous voxels obtained along the line of 80 voxels at a given location. For example, to obtain 40 waveforms based on the average of 40 contiguous voxels, we averaged voxels 1 through 40, 2 through 41, 3 through 42, and so on, over the 80 voxels available that have the same theoretical displacement. The largest peak-to-peak difference among the 40 DENSE MRI waveforms compared with LDV was then obtained. This method was repeated for 20, 10, 5, and 2 contiguous voxels to determine the impact of averaging on displacement accuracy.

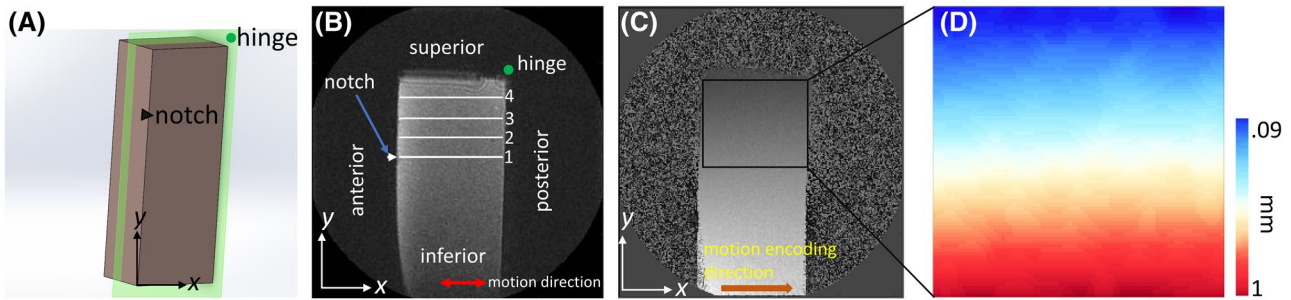


FIGURE 3 Displacement-encoding with stimulated echoes (DENSE) MR images of a tissue phantom. A, Simulated tissue phantom showing MRI scan plane. B, Magnitude image. Numbers 1, 2, 3, and 4, represent the locations where the laser Doppler vibrometer measurements were performed, white lines show the row of averaged voxels, and red arrows show the direction of tissue phantom motion). C, Phase image at peak displacement (black box indicates the region of interest). D, Two-dimensional pixel-wise Eulerian displacement. (Note: In Figure 3B, the green dot represents the location of the hinge, and in Figure 3C, the brown arrow represents the motion-encoding direction)

TABLE 1 Cycle-to-cycle, before/after MRI consistency, and comparison of DENSE and LDV displacement waveforms with different peak displacements

Peak (mm)	Cycle-to-cycle consistency		Before/after MRI			DENSE vs LDV		
	Range of diff (μm)	Max RMSE (μm)	Peak-to-peak diff (μm)	Range of diff (μm)	RMSE (μm)	Peak-to-peak diff (μm)	Range of diff (μm)	RMSE (μm)
1.04	-13 to 13	9	8	-9 to 24	11	18	-12 to 50	19
0.76	-8 to 10	5	5	-7 to 14	6	14	-10 to 41	10
0.55	-7 to 5	3	0	-15 to 7	5	1	-12 to 26	17
0.22	-3 to 4	2	5	-10 to 3	5	7	-14 to 15	9

Abbreviations: DENSE, displacement-encoding with stimulated echoes; LDV, laser Doppler vibrometer; RMSE, root mean square error.

3 | RESULTS

3.1 | LDV consistency: Cycle-to-cycle and before/after MRI

To determine the cycle-to-cycle consistency of the LDV displacement waveforms, the ensemble average displacement waveform was compared with the 180 individual displacement waveforms (Figure 2B). At the location on the moving plate with the peak displacement of 1.04 mm (location 1 on Figure 3B), the minimum and maximum cycle-to-cycle displacement difference recorded was -13 and $+13$ μm , respectively, whereas the RMSE was 9 μm (see Table 1). The LDV cycle-to-cycle consistency was determined for 3 additional locations with a peak displacement of 0.76, 0.55, and 0.22 mm (locations 2, 3, and 4 in Figure 3B, respectively).

To determine the disconnection/reconnection repeatability, 2 ensemble average displacement reference waveforms (before and after DENSE MRI measurements) were compared for the 4 locations on the moving tissue phantom. At the location with a peak displacement of 1.04 mm, the peak-to-peak difference, minimum difference, maximum difference, and RMSE before and after MRI measurement were 8, -9 , 24, and 11 μm , respectively, as shown in Figure 4A (see Figure 4B-D and Table 1 for the repeatability results at the other 3 locations).

3.2 | Comparison of DENSE MRI and LDV displacement waveforms

The displacement obtained with DENSE MRI was compared with the reference displacement obtained with the LDV at 4 different locations (peak displacements of 1.04, 0.76, 0.55, and 0.22 mm). At a peak displacement of 1.04 mm, the peak-to-peak difference, minimum difference, maximum difference, and RMSE between the DENSE MRI and LDV were 18, -12 , 50, and 19 μm , respectively, as shown in Figure 5A (see Figure 5B-D and Table 1 for the results of the 3 additional locations). Reducing the distance between the point of LDV measurement and the hinge (radius) results in a linear reduction in the peak displacements (Figure 6).

3.3 | Effect of voxel-averaging on the DENSE MRI displacement waveform

The peak-to-peak difference between DENSE and LDV for the average of 80 voxels was 18 μm for 1.04-mm peak displacement. Averaging smaller collections of contiguous voxels gave larger peak-to-peak difference values. The maximum peak-to-peak difference for 40, 20, 10, 5, and 2 averaged voxels were 24, 26, 31, 31, and 32 microns, respectively

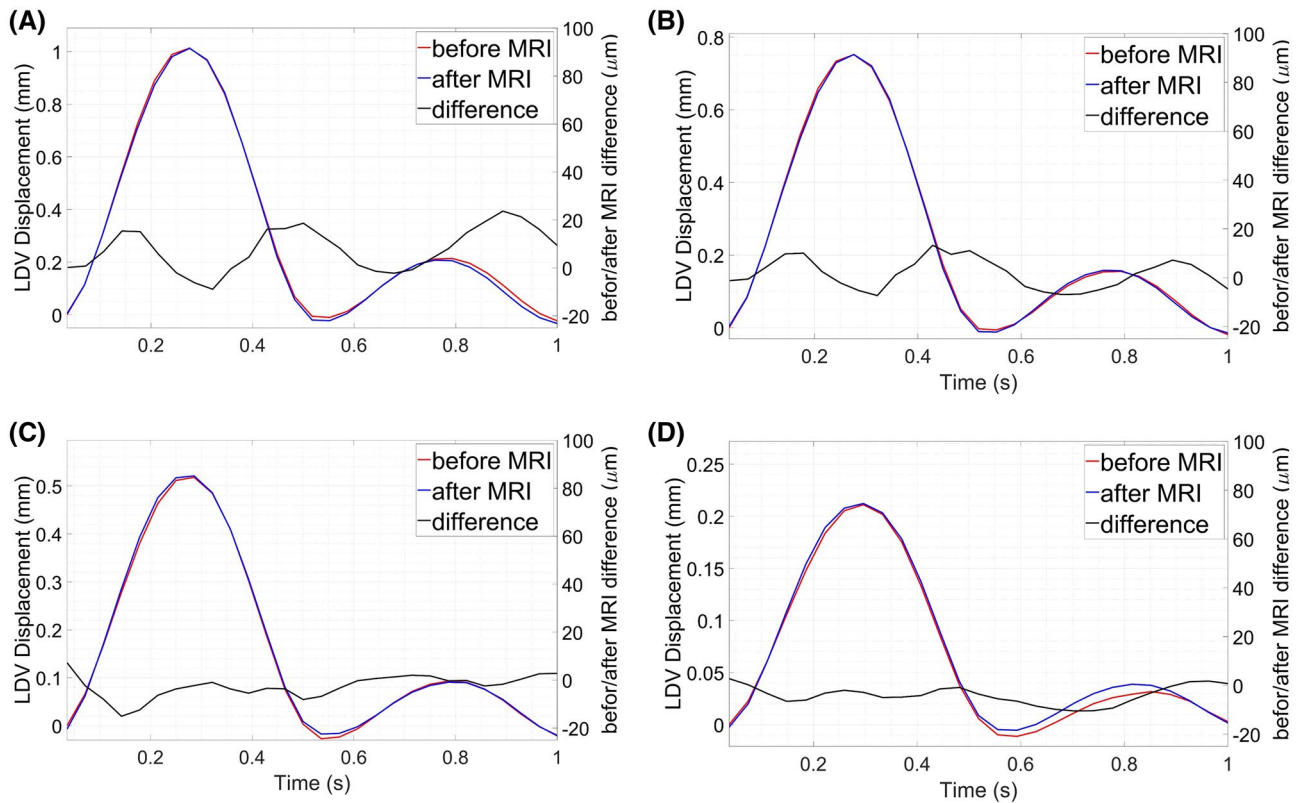


FIGURE 4 Comparison of laser Doppler vibrometer displacement reference waveform before and after displacement-encoding with stimulated echoes magnetic resonance imaging measurements at peak displacements of (A) 1.04, (B) 0.76, (C) 0.55, and (D) 0.22 mm. Although the ordinate is shown with the same scale in all subfigures, the scale for the abscissa is adjusted in each subfigure based on the above-mentioned peak displacement. Note: waveforms a, b, c, and d were measured at locations 1, 2, 3, and 4, respectively, shown in Figure 3B

(see Table 2). Similar results were obtained at 3 different locations with a peak displacement of 0.76, 0.55, and 0.22 mm (see Table 2). For a displacement waveform with peak displacement of 220 μm , averaging 80 voxels resulted in a peak-to-peak displacement error of 3%; this error was further improved as a percentage when the peak displacement increased to 1.04 mm dropping to 1.7%. Although we found the average of 80 voxels to provide the most accurate measurement of displacement between DENSE MRI compared with LDV, averaging smaller numbers of voxels also produced good results (for a waveform with a peak displacement of 220 μm , the average of 40, 20, 10, 5, and 2 voxels resulted in a maximum peak-to-peak displacement error of 8.6%, 11.4%, 12.7%, 14.1%, and 14.5%, respectively). For a 1.04-mm peak displacement, averaging smaller numbers of voxels also produced lower displacement errors (averaging 40, 20, 10, 5, and 2 voxels resulted in a maximum peak-to-peak displacement error of 2.3%, 2.5%, 3.0%, 3.0%, and 3.1%, respectively).

4 | DISCUSSION

The results of this study demonstrated high accuracy of DENSE MRI in measuring displacements representative of

cardiac-induced brain tissue motion (peak-to-peak error of 7 μm for a displacement waveform with a peak of 220 μm). Therefore, we conclude that DENSE MRI can be considered an accurate technique for characterizing human brain tissue motion.

Previous phantom studies with myocardial tagging have been used to track the motion of the heart.^{32,33} These studies reported tracking accuracies of up to 270 μm between the displacement measured with phantom designs compared with myocardial tagging. Using DENSE MRI, Spottiswoode et al compared a typical cardiac displacement to a displacement obtained with a rotating phantom. They reported a displacement error of $240 \pm 150 \mu\text{m}$.²⁷ This error represents between 2.4%–4% of the maximum cardiac displacement (cardiac displacement has been reported to be between 6–10 mm³⁰). Although this displacement error (240 μm) is acceptable for cardiac displacement, it is higher than the maximum average displacement reported for healthy brain tissue (100–187 μm).^{12,13} In this study, we compared the displacement from DENSE to that of LDV in 4 locations on the moving plate with peak displacement ranging from 1.04 mm to 0.22 mm. Peak displacements of 1.04 mm and 0.22 mm represent in vivo brain tissue displacement reported for pathological³⁴ and healthy subjects¹², respectively. The results we obtained were comparable to that of Spottiswoode et al on a

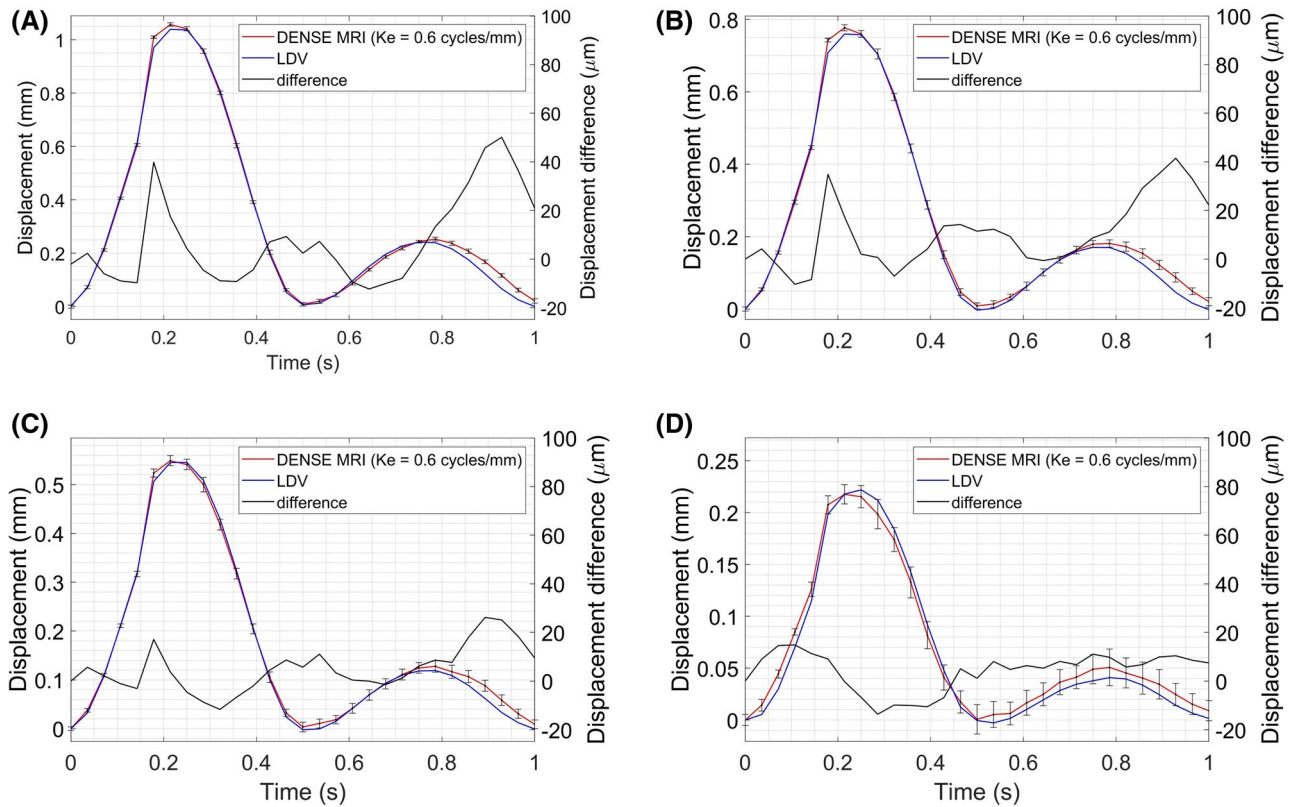


FIGURE 5 Comparison between displacement-encoding with stimulated echoes magnetic resonance imaging (DENSE MRI) and laser Doppler vibrometer (LDV) at peak displacement of (A) 1.04, (B) 0.76, (C) 0.55, and (D) 0.22 mm. Note: waveforms a, b, c, and d were derived from locations 1, 2, 3, and 4, respectively, shown in Figure 3B. Error bars show the SD across 80 rows of voxels with similar displacement values from the anterior to the posterior section of the tissue phantom shown in Figure 3B

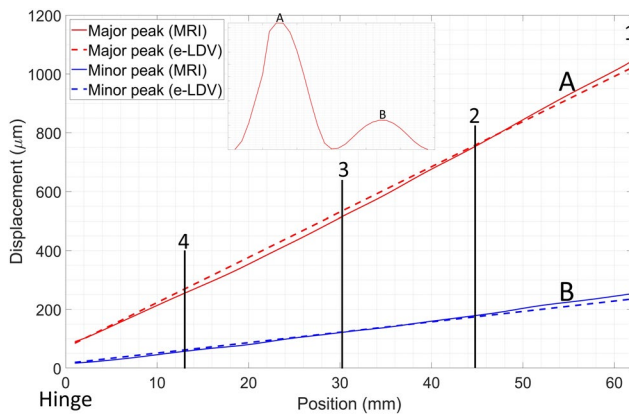


FIGURE 6 Change in displacement-encoding with stimulated echoes magnetic resonance imaging (DENSE MRI) displacement over tissue length. (Note: In this figure, A = major peak, B = minor peak. The estimated laser Doppler vibrometer (e-LDV) was derived by extrapolating the linear fit of the 4 LDV measurements performed at locations 1, 2, 3, and 4. The black lines with numbers 1, 2, 3, and 4 represent the location where the LDV measurement with peak displacement of 1.04, 0.76, 0.55, and 0.22 mm were performed, respectively)

percentage basis, as we found a maximum displacement error of 50 μm for a peak displacement of 1.04 mm (4.8% displacement error) using DENSE MRI. Peak-to-peak displacement showed

a lower displacement error between DENSE MRI and LDV (18 μm or 1.7% displacement error for the waveform with a peak of 1.04 mm). Phantom studies have also been used to validate displacement derived from velocity-encoding techniques.¹⁶⁻¹⁸ Zhu et al reported a displacement error of 0.92 mm (4.6%) for a maximum displacement of 19.8 mm using a compensated Fourier integration technique. However, this group did not examine small displacements representative of those observed in the brain tissue.³⁵

Both DENSE MRI and PCMRI have been used for characterizing neural tissue motion. Several researchers have characterized neural tissue displacement from PCMRI by integrating the velocity of the tissue motion over the cardiac cycle.¹⁹⁻²⁵ Because PCMRI measures velocity directly, it can only provide an indirect measurement of displacement, where the integration of velocity over the cardiac phase could potentially accumulate errors in each cardiac phase. In contrast, DENSE MRI measures the displacement of each cardiac phase independently, and therefore result in no integration-induced accumulated errors. Compared with other motion measurement techniques such as tissue tagging or cine imaging, DENSE MRI has the advantage of encoding displacements at a much smaller magnitude than the pixel resolution of the image.^{1,4,11,12}

TABLE 2 Effect of voxel averaging on the peak-to-peak difference between DENSE MRI and LDV waveforms

Number of voxels averaged	Max peak-to-peak difference (μm) between DENSE MRI and LDV			
	Peak of 1.04 mm	Peak of 0.76 mm	Peak of 0.55 mm	Peak of 0.22 mm
80	18	14	1	7
40	24	25	9	19
20	26	26	16	25
10	31	32	20	28
5	31	33	23	31
2	32	33	26	32

Abbreviations: DENSE, displacement-encoding with stimulated echoes; LDV, laser Doppler vibrometer.

Brain tissue motion in pathological conditions such as Chiari malformation has been reported to be up to 1 mm.³⁴ The variation in displacement in the 80 voxels with the same displacement is given by the error bars in Figure 5. Selecting a single voxel to determine the displacement in areas of the brain with tissue displacement of 1 mm (as seen in subjects with Chiari malformation), may not result in large errors (see Figure 5A). However, in situations where the tissue displacement is lower than 250 μm as reported for healthy individuals,¹² relying on a single voxel may result in significant errors in the displacement measurement (see Figure 5D).

This study had limitations. The notch on the tissue phantom was manually created and was used to determine the coincident location of the LDV and DENSE MRI measurements. The reflective tape was manually placed coincident with the notch and the LDV laser beam was manually focused at the center of the reflective tape. Thus, the location of the LDV measurement could be erroneously offset by approximately 130 μm relative to the notch. Through trigonometry, the LDV peak displacement error caused by this offset is computed to be approximately 2 μm . Furthermore, the phantom was not made of living tissues, and thus, had different MRI properties (for example, T_1/T_2 relaxation times and diffusion properties) compared with that of the brain tissue of a living subject. We did not employ any FA sweep in the current study. The sequence, as implemented on our scanner, did not allow for the use of a ramped FA to reduce the T_1 decay effect. Future studies will focus on investigating the effect of ramped FA on the DENSE scans. Additionally, the images of the phantom were acquired near the isocenter and the center of the head coil. The size of the phantom and location of measurements ensured that measurements were made near the isocenter, resulting in the very small background offset in the no motion scan (3 μm)—indicating that the Maxwell terms were small. However, for larger structures such as the brain, larger background offsets may be seen, and thus, may require correcting. The heart rate employed in this study was 60 beats per minute;

therefore, error estimates may not be similar in subjects with a higher heart rate. The external trigger was created using an ultrasonic sensor, and the delay between cycles was demonstrated to be on the order of 1 ms. This delay is not expected to cause errors at the peaks in the displacement curve (positions A and B, Figure 6). However, with maximum tissue velocity estimated to be approximately 3 $\mu\text{m}/\text{ms}$ (position A, Figure 6), a 1-ms delay could result in a displacement error of approximately 3 μm .

5 | CONCLUSIONS

To conclude, this study demonstrated that DENSE MRI is capable of measuring brain tissue displacements accurately, for waveforms similar in magnitude and frequency to those observed in healthy brain tissue. The importance of brain tissue motion has yet to be uncovered. However, it may be possible to differentiate healthy and pathological tissue for many brain disorders, such as Chiari malformation, hydrocephalus, dementia, cancerous tumors, and traumatic brain injury. The utility of DENSE MRI to accurately measure displacements on the scale of microns might be promising for potential brain tissue applications.

ACKNOWLEDGMENTS

The authors would like to thank Conquer Chiari and the National Institutes of Health, NINDS R15 (Grant No. 1R15NS109957-01A1) for providing funding for this research work. This work was also supported by the National Center for Advancing Translational Sciences of the National Institutes of Health under award number UL1TR002378. The educational material is based upon work supported by the National Science Foundation under NSF CAREER Award No. 1846715.

CONFLICT OF INTEREST

Xiaodong Zhong is a Siemens employee.

ORCID

Blaise Simplicie Talla Nwotchouang  <https://orcid.org/0000-0002-2479-0903>

Xiaodong Zhong  <https://orcid.org/0000-0001-8355-5279>

TWITTER

Blaise Simplicie Talla Nwotchouang  @chingling_20

REFERENCES

- Aletras AH, Ding S, Balaban RS, Wen H. DENSE displacement encoding with stimulated echoes in cardiac functional MRI. *J Magn Reson*. 1999;137:247-252.
- Zhong X, Spottiswoode BS, Meyer CH, Kramer CM, Epstein FH. Imaging three-dimensional myocardial mechanics using navigator-gated volumetric spiral cine DENSE MRI. *Magn Reson Med*. 2010;64:1089-1097.
- Kim D, Gilson WD, Kramer CM, Epstein FH. Myocardial tissue tracking with two-dimensional cine displacement-encoded MR imaging: Development and initial evaluation. *Radiology*. 2004;230:862-871.
- Zhong X, Meyer CH, Schlesinger DJ, et al. Tracking brain motion during the cardiac cycle using spiral cine-DENSE MRI. *Med Phys*. 2009;36:3413-3419.
- Wehner GJ, Jing L, Haggerty CM, et al. Comparison of left ventricular strains and torsion derived from feature tracking and DENSE CMR. *J Cardiovasc Magn Reson*. 2018;20:63.
- Iffrig E, Wilson JS, Zhong X, Oshinski JN. Demonstration of circumferential heterogeneity in displacement and strain in the abdominal aortic wall by spiral cine DENSE MRI. *J Magn Reson Imaging*. 2019;49:731-743.
- Wilson JS, Taylor WR, Oshinski J. Assessment of the regional distribution of normalized circumferential strain in the thoracic and abdominal aorta using DENSE cardiovascular magnetic resonance. *J Cardiovasc Magn Reson*. 2019;21:59-59.
- Feinberg DA, Mark AS. Human brain motion and cerebrospinal fluid circulation demonstrated with MR velocity imaging. *Radiology*. 1987;163:793-799.
- Greitz D, Franck A, Nordell B. On the pulsatile nature of intracranial and spinal CSF-circulation demonstrated by MR imaging. *Acta Radiol*. 1993;34:321-328.
- Reese TG, Feinberg DA, Dou J, Wedeen VJ. Phase contrast MRI of myocardial 3D strain by encoding contiguous slices in a single shot. *Magn Reson Med*. 2002;47:665-676.
- Soellinger M, Rutz AK, Kozerke S, Boesiger P. 3D cine displacement-encoded MRI of pulsatile brain motion. *Magn Reson Med*. 2009;61:153-162.
- Pahlavian SH, Oshinski J, Zhong X, Loth F, Amini R. Regional quantification of brain tissue strain using displacement-encoding with stimulated echoes magnetic resonance imaging. *J Biomech Eng*. 2018;140:17-1563.
- Adams AL, Kuijff HJ, Viergever MA, Luijten PR, Zwanenburg JJM. Quantifying cardiac-induced brain tissue expansion using DENSE. *NMR Biomed*. 2019;32:e4050.
- Adams AL, Viergever MA, Luijten PR, Zwanenburg JJM. Validating faster DENSE measurements of cardiac-induced brain tissue expansion as a potential tool for investigating cerebral microvascular pulsations. *NeuroImage*. 2020;208:116466.
- Sloots JJ, Biessels GJ, Zwanenburg JJM. Cardiac and respiration-induced brain deformations in humans quantified with high-field MRI. *NeuroImage*. 2020;210:116581.
- Constable RT, Rath KM, Sinusas AJ, Gore JC. Development and evaluation of tracking algorithms for cardiac wall motion analysis using phase velocity MR imaging. *Magn Reson Med*. 1994;32:33-42.
- Drangova M, Zhu Y, Bowman B, Pelc NJ. In vitro verification of myocardial motion tracking from phase-contrast velocity data. *Magn Reson Imaging*. 1998;16:863-870.
- Pelc NJ, Drangova M, Pelc LR, et al. Tracking of cyclic motion with phase-contrast cine MR velocity data. *J Magn Reson Imaging*. 1995;5:339-345.
- Alperin N, Loftus JR, Oliu CJ, et al. Magnetic resonance imaging measures of posterior cranial fossa morphology and cerebrospinal fluid physiology in Chiari malformation Type I. *Neurosurgery*. 2014;75:515-522.
- Hofmann E, Warmuth-Metz M, Bendszus M, Solymosi L. Phase-contrast MR imaging of the cervical CSF and spinal cord: Volumetric motion analysis in patients with Chiari I malformation. *Am J Neuroradiol*. 2000;21:151.
- Lawrence BJ, Luciano M, Tew J, et al. Cardiac-related spinal cord tissue motion at the Foramen Magnum is increased in patients with type I Chiari malformation and decreases postdecompression surgery. *World Neurosurg*. 2018;116:e298-e307.
- Noam A, Anusha S, Terry L. Magnetic resonance imaging—Based measurements of cerebrospinal fluid and blood flow as indicators of intracranial compliance in patients with Chiari malformation. *J Neurosurg*. 2005;103:46-52.
- Pujol J, Roig C, Capdevila A, et al. Motion of the cerebellar tonsils in Chiari type I malformation studied by cine phase-contrast MRI. *Neurology*. 1995;45:1746-1753.
- Sivaramakrishnan A, Alperin N, Surapaneni S, Lichtor T. Evaluating the effect of decompression surgery on cerebrospinal fluid flow and intracranial compliance in patients with Chiari malformation with magnetic resonance imaging flow studies. *Neurosurgery*. 2004;55:1344-1351.
- Wolpert SM, Bhadelia RA, Bogdan AR, Cohen AR. Chiari I malformations: Assessment with phase-contrast velocity MR. *Am J Neuroradiol*. 1994;15:1299-1308.
- Greitz D, Wirestam R, Franck A, Nordell B, Thomsen C, Ståhlberg F. Pulsatile brain movement and associated hydrodynamics studied by magnetic resonance phase imaging. *Neuroradiology*. 1992;34:370-380.
- Spottiswoode BS, Zhong X, Hess AT, et al. Tracking myocardial motion from cine DENSE images using spatiotemporal phase unwrapping and temporal fitting. *IEEE Trans Med Imaging*. 2007;26:15-30.
- Young AA, Li B, Kirton RS, Cowan BR. Generalized spatiotemporal myocardial strain analysis for DENSE and SPAMM imaging. *Magn Reson Med*. 2012;67:1590-1599.
- Kim D, Epstein FH, Gilson WD, Axel L. Increasing the signal-to-noise ratio in DENSE MRI by combining displacement-encoded echoes. *Magn Reson Med*. 2004;52:188-192.
- Tan W, Xu L, Wang X, Qiu D, Han G, Hu D. Estimation of the displacement of cardiac substructures and the motion of the coronary arteries using electrocardiographic gating. *Oncotargets Ther*. 2013;6:1325-1332.
- Zhong X, Spottiswoode BS, Cowart EA, Gilson WD, Epstein FH. Selective suppression of artifact-generating echoes in cine DENSE using through-plane dephasing. *Magn Reson Med*. 2006;56:1126-1131.
- McVeigh ER, Zerhouni EA. Noninvasive measurement of transmural gradients in myocardial strain with MR imaging. *Radiology*. 1991;180:677-683.

33. Young AA, Kraitchman DL, Dougherty L, Axel L. Tracking and finite element analysis of stripe deformation in magnetic resonance tagging. *IEEE Trans Med Imaging*. 1995;14:413-421.
34. Leung V, Magnussen JS, Stoodley MA, Bilston LE. Cerebellar and hindbrain motion in Chiari malformation with and without syringomyelia. *J Neurosurg-Spine*. 2016;24:546-555.
35. Zhu Y, Drangova M, Pelc NJ. Fourier tracking of myocardial motion using cine-PC data. *Magn Reson Med*. 1996;35:471-480.

SUPPORTING INFORMATION

Additional Supporting Information may be found online in the Supporting Information section.

FIGURE S1 Schematic of the tissue phantom on the moving bed. Voxel averaging was conducted along the vertical direction

(eg, along the line AB). Theoretically, at each given time point t , when the hinge has the angle $\alpha(t)$ with the horizontal axis and the moving bed has the angular velocity of $\omega(t)$, the voxels along any vertical line should have the same velocity values

How to cite this article: Nwotchouang BST, Eppelheimer MS, Biswas D, et al. Accuracy of cardiac-induced brain motion measurement using displacement-encoding with stimulated echoes (DENSE) magnetic resonance imaging (MRI): A phantom study. *Magn Reson Med*. 2021;85:1237–1247. <https://doi.org/10.1002/mrm.28490>